ChemPubSoc Europe

DOI: 10.1002/cbic.201900261

CHEMBIOCHEM Full Papers

Effect of UV Radiation on Fluorescent RNA Aptamers' Functional and Templating Ability

Ranajay Saha[a] and Irene A. Chen*[a, b, c]

Damage from ultraviolet (UV) radiation was likely to be an important selection pressure during the origin of life. RNA is believed to have been central to the origin of life and might form the basis for simple synthetic cells. Although photodamage of DNA has been extensively studied, photodamage is highly dependent on local molecular context, and damage to functional RNAs has been relatively under-studied. We irradiated two fluorescent RNA aptamers and monitored the loss of activity, folding, and the kinetics of lesion accumulation. The loss of activity differed depending on the aptamer, with the Spinach2 aptamer retaining substantial activity after long exposure times. The binding pocket was particularly susceptible to damage, and melting of the duplex regions increased susceptibility; this is consistent with the view that duplex formation is protective. At the same time, susceptibility varied greatly depending on context, thus emphasizing the importance of studying many different RNAs to understand UV hardiness.

Introduction

One approach to building a bottom-up synthetic cell finds inspiration from the origin of life. In particular, the dual nature of RNA suggests that the complexities of implementing the central dogma of molecular biology could be avoided by using RNA as both genetic carrier and functional molecules, and thus an early RNA World has been proposed as a simpler precursor to more modern cells.[1] Intriguing prebiotic syntheses of ribonucleotides,[2] amino acids,[3] and even iron–sulfur clusters[4] rely on reactions driven by UV radiation. Indeed, UV radiation might have been the largest source of energy available for prebiotic chemistry.[5] Even if UV radiation were not involved in prebiotic reactions, the surface of the early Earth was subject to two to three orders of magnitude more radiative flux near the absorption peak of the nucleobases compared to the present-day Earth, primarily due to the altered composition of the atmosphere.[6] In particular, the UV fluence of the early Earth was estimated to be $\approx 4\times10^{13}$ photons s^{-1} cm^{-2} near the $\pi\pi^*$ absorption peak of nucleobases (250–260 nm) and $\approx 10^{15}$ photons s^{-1} cm^{-2} in the UVC range of 200–300 nm.[5] The damage resulting from high levels of UV exposure could have represented an important physical selection on the chemical constituents of prebiotic systems.[7] Thus, understanding the effect of UV radiation on RNA is important for understanding the potential for emergence of an RNA World on the early Earth. In addition, practical methods for UV disinfection of RNA-based viral pathogens, as well as efforts to build a synthetic cell that would eventually be exposed to the Earth's surface, might benefit from an improved understanding of the effects of UV damage on RNA.

Previous studies on UV-induced RNA damage, reviewed elsewhere,[8] show that, as with DNA, the formation of cyclobutane pyrimidine dimers is a dominant lesion. In addition, adenine cycloaddition to T or A results in lesions at TA or AA sites.[9] Indeed, UV exposure is an established technique for RNA–RNA crosslinking to identify sites in close proximity in a tertiary or quaternary structure.[10] Single bases are also prone to damage, particularly UV-induced photooxidation of G to produce 8-oxo-G, as well as photohydration of pyrimidines to form uracil or cytosine hydrate.[11]

In general, the aromatic rings of the nucleobases absorb photons in the UV range, resulting in an excited electronic state. The excited state is highly reactive and can give rise to chemical lesions, and thus the lifetime of the excited state largely determines the propensity of a particular nucleobase to UV-induced damage. Exit from the excited state can occur by relatively slow radiative processes (e.g., fluorescence, which occurs on the nanosecond timescale) or by faster nonradiative processes, such as internal conversion to the electronic ground state (which occurs on a picosecond timescale). Internal con-

[a] Dr. R. Saha, Prof. I. A. Chen
Department of Chemistry and Biochemistry, University of California
Santa Barbara, CA 93106 (USA)
E-mail: chen@chem.ucsb.edu

[b] Prof. I. A. Chen
Program in Biomolecular Sciences and Engineering, University of California
Santa Barbara, CA 93106 (USA)

[c] Prof. I. A. Chen
Department of Chemical and Biomolecular Engineering
University of California
Los Angeles, CA 90095 (USA)

Supporting information and the ORCID identification numbers for the authors of this article can be found under https://doi.org/10.1002/cbic.201900261.

This article is part of a Special Issue on Bottom-up Synthetic Biology.

version involves flexion of the molecular structure to a conformation at which the energy of the excited state is close to the energy of an intermediate state or the ground state (forming a "conical intersection"), thus allowing crossover to the ground state and dissipation of the energy as heat to the environment. Therefore, the rate of internal conversion, and thus the lifetime the excited state, is highly sensitive to the molecular context of the nucleobases, including base pairing, π stacking, and solvation.[12] For example, in the gas phase, the Watson–Crick GC base pair exhibits faster internal conversion than other possible GC clusters.[13] However, steric hindrance within a molecular context can impede the out-of-plane motion required to access the conical intersections; ss- and dsDNAs have excited-state lifetimes that are two to three orders of magnitude longer than those of monomers.[12b] In one early study, poly(U) was found to be five to ten times more prone to UV damage than a 1:1 mixture of poly(A) and poly(U), thus indicating that the double-stranded structure was protective.[14] Solvent conditions are also important, as tobacco mosaic virus (TMV) RNA was shown to accumulate lesions more slowly in the presence of 1 mM Mg^{2+}, possibly due to improved folding. Another difference found was that dimers predominate among chemical lesions in the presence of Mg^{2+}, whereas hydrates predominate without it.[15] A designed series of hairpin oligonucleotides illustrated the sometimes surprising sensitivity to structure and conformation,[16] as well as the increased UV hardiness of A-form RNA compared to B-form DNA; this has also been observed in a comparison of viral genomes.[17]

Due to this context sensitivity, studies in the gas phase or with model oligonucleotides are difficult to extend to functional RNAs, which adopt complex, specific three-dimensional folds. In addition, studies of substituent and solvent effects suggest the presence of additional "dark" excited states whose properties might be difficult to predict from a theoretical basis.[18] Therefore, empirical studies on specific systems are important in order to understand their UV hardiness. Prior studies on functional RNAs illustrate loss of function upon UV exposure. For example, UV radiation induced a long-range crosslink in tRNA in vivo between cytidine and 4-thiouridine that resulted in inefficient aminoacylation and amino acid incorporation.[19] This particular lesion is consistent with the general finding that the canonical nucleobases have shorter excited-state lifetimes than modified nucleobases, suggestive of a photochemical selection of nucleobases on the early Earth.[12a] UV exposure of rRNA in vivo showed that adjacent pyrimidines were primarily affected; this is consistent with pyrimidine dimers. Interestingly, the ribosomal active site was particularly affected, resulting in decreased translation activity.[20] However, these in vivo studies might not mimic an RNA World cell, as modern cells possess multiple mechanisms for DNA and RNA repair.[8] Indeed, higher-order structures and solution composition play a significant role, with repair mechanisms being strongly influenced by nucleosome structure and positioning.[21] One study of a hairpin ribozyme exposed to UV in vitro showed a roughly 50% decrease in activity upon UV exposure, with the presence of montmorillonite clay being protective;[22] the mechanism of this effect and the degree of UV exposure were unknown.

In this work, we studied empirically how UV radiation would affect the function and replicability of RNA aptamers under dilute conditions in vitro. We expose two RNA aptamers, the malachite green (MG) aptamer and the Spinach2 aptamer, to UV radiation at an overall fluence comparable to that of the early Earth. These aptamers were chosen because their structures have previously been characterized, thus facilitating the interpretation of chemical lesions, and because their phenotypes are readily assayed by fluorescence.[23] We characterized the resulting loss of activity over time, assayed the templating ability of the RNA by reverse transcription, and determined the location of major chemical lesions. Although these aptamers are products of in vitro selection rather than natural evolution, the results could inform the understanding of factors that influenced the lifetimes of functional RNA on the surface of the prebiotic Earth.

Results

Loss of activity of RNA aptamers upon UV exposure

Two RNA aptamers were studied: the MG aptamer and the Spinach2 aptamer (which binds DHFBI and its derivatives, including DHFBI 1T); each aptamer binds a small-molecule dye that is essentially nonfluorescent in free solution but increases greatly in fluorescence when bound by the RNA aptamer.[24] The fluorescence of the dye·aptamer complex was used to monitor the effect of UV radiation on the activity of the RNA. The dye was added to the RNA after UV exposure for a given period of time in order to avoid effects due to irradiation of the dye itself; nevertheless, irradiation in the presence of MG dye showed a roughly similar rate of loss of overall fluorescence (Figure S1 A in the Supporting Information).

For the MG aptamer, the fluorescence of the aptamer·dye complex decreased as UV exposure time increased, decaying exponentially with a rate constant of $0.76 \pm 0.01\ h^{-1}$, to a final fluorescence of $5 \pm 1\%$ of the initial fluorescence at long times (Figure 1 A). Without irradiation, the MG aptamer demonstrated no detectable loss of fluorescence over the same time (Figure S1 B). For Spinach2, an exponential decrease of fluorescence was also observed upon UV radiation, with a somewhat slower rate of damage ($0.40 \pm 0.08\ h^{-1}$). Interestingly, the final fluorescence after long UV exposure times was notably high ($25 \pm 3\%$) for the Spinach2 aptamer compared to the MG aptamer. To determine whether the rate of activity loss depended on the folding of the RNA, we irradiated the MG aptamer at 80 °C, which is well above the melting point (see also Figure 2 B, below).[25] No significant change in rate or final fluorescence was observed ($1.0 \pm 0.2\ h^{-1}$ and $4 \pm 1\%$, respectively; Figure 1 B), thus indicating that the folded and unfolded states of this aptamer are similarly susceptible to activity loss through UV damage. We also tested whether encapsulation of the MG aptamer inside phospholipid vesicles (composed of 1-palmitoyl-2-oleoyl-glycero-3-phosphocholine (POPC)), which promotes aptamer folding,[25] affected the rate of activity loss. Encapsulation did not significantly affect the rate of loss of fluo-

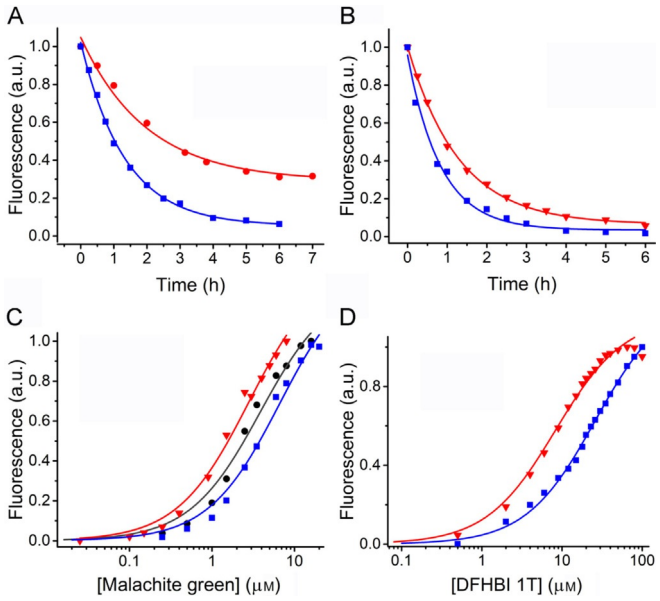

Figure 1. Loss of RNA aptamer binding activity from UV exposure. A) Normalized fluorescence of the MG (■) and Spinach2 (●) aptamers upon varying time of UV exposure. B) Normalized fluorescence of the MG aptamer during UV exposure at room temperature (▼) or 80 °C (■). C) Binding curve of the MG aptamer after 0 (▼; $K_D = 2.4 \pm 0.3$ μM), 1.8 (●; $K_D = 3.6 \pm 0.2$ μM), or 6 (■; $K_D = 5.7 \pm 0.5$ μM) hours of UV exposure. D) Binding curve of the Spinach2 aptamer after 0 (▼; $K_D = 8 \pm 0.2$ μM) or 6 h (■; $K_D = 27 \pm 3$ μM) of UV exposure.

rescence (Figure S1 C); however, exposure at lower UV fluence resulted in less loss of fluorescence, as expected (Figure S1 D).

In general terms, a loss of bulk fluorescence could be caused by a reduction in the number of functional molecules, to leave a subset of active molecules, or by a more uniform decline in the activity of the molecules. If the loss of fluorescence were caused by a reduction in the number of functional molecules, the apparent K_D measured for the RNA would not be greatly altered from that of unexposed RNA. On the other hand, if the loss of fluorescence were caused by a more uniform decline in the activity of the molecules, the apparent K_D would show decreased affinity. For the MG aptamer, the K_D increased only slightly (≈threefold) with UV exposure (Figure 1 C), thus indicating that the remaining fluorescence of the population is due to functionally intact molecules. Similarly, the increase in the K_D value was modest for the Spinach2 aptamer after UV damage (≈threefold; Figure 1 D). This pattern suggests that the aptamer population consists of two types of molecule after UV exposure: those that have little or no activity, and those that are largely functionally intact.

Effect of UV exposure on the structural stability of the aptamers

To determine how UV exposure affects the structural stability of the aptamers, we measured the melting transition of the MG-bound aptamer by fluorescence; this reports on local structural changes in the ligand-binding site. The transition temperature (T_t) of the MG aptamer was 34.2 ± 2.3 °C without irradiation, but was reduced to 11.9 ± 0.9 °C after 6 h of UV exposure (Figure 2 A), thus indicating that, although a subpopulation of fluorescent molecules has roughly normal affinity, the structural stability of the binding site is impaired by UV damage. To monitor the global stability of the RNA secondary structure, we also monitored the melting temperature by CD spectroscopy. The CD spectrum of the MG aptamer has a characteristic peak at 264 nm, whose ellipticity is slightly decreased after UV irradiation for 6 h (Figure S1 E). The overall T_m of the MG aptamer monitored by CD was 71 ± 2 °C before UV irradiation and 74 ± 3 °C after UV treatment for 6 h (Figure 2 B). Thus, in contrast to the sensitivity of local structural stability (T_t) to UV exposure, overall stability (T_m) of the MG aptamer was not affected by UV exposure. In contrast to the MG aptamer, the Spinach2 aptamer did not show a difference in T_t measured by fluorescence (Figure 2 C), thus indicating that UV damage to the Spinach2 aptamer does not affect the stability of the ligand-binding site.

The melting studies indicated that local interactions in the binding pocket of the MG aptamer were disrupted by UV exposure, although global secondary structure seemed to be intact. To better understand the effect of UV exposure on RNA folding, the UV-treated MG aptamer was analyzed by native and denaturing polyacrylamide gel electrophoresis. Under denaturing conditions, no changes in the banding pattern were observed for the UV-treated sample, thereby confirming that the RNA backbone was intact, as expected (Figure 3 A).[12a,22] However, the native gel revealed additional slowly migrating conformers in the UV-treated sample (Figure 3 B), thus indicat-

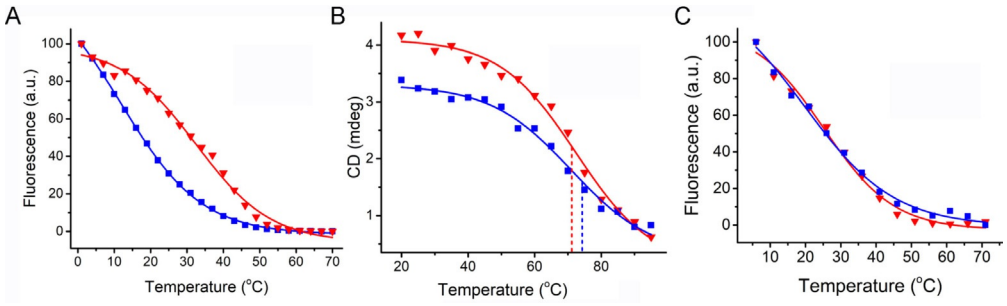

Figure 2. Effect of UV exposure on the melting transition of aptamers. The melting curves are shown before (▼) or after (■) 6 h of exposure to UV irradiation. The MG aptamer was monitored by A) fluorescence and B) CD spectroscopy. C) The transition of the Spinach2 aptamer shows no significant change before (▼; $T_t = 24$ and 25 °C for duplicates) and after (■; $T_t = 20$ and 26 °C for duplicates) UV irradiation.

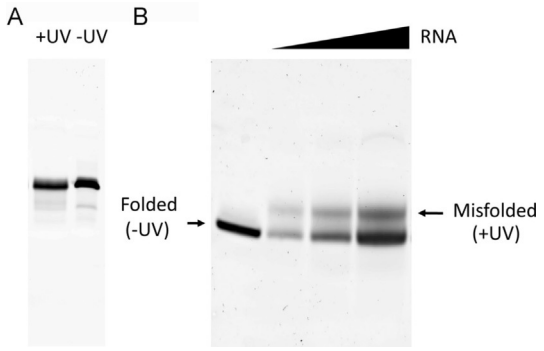

Figure 3. Partial unfolding of a UV-damaged MG aptamer. A) Denaturing PAGE of the MG aptamer after exposure to UV for 6 h (+UV) or incubated in the dark for 6 h (−UV). B) Native PAGE of the MG aptamer, without exposure (incubated in the dark for 6 h, left) or with exposure (right 3 lanes, with increasing amount of loaded RNA) to UV for 6 h, illustrating the presence of a more slowly migrating band after irradiation. Irradiated samples were ethanol-precipitated and annealed before native PAGE.

ing misfolded RNA molecules. The position of the new band is qualitatively consistent with misfolding of the MG aptamer from UV damage, as suggested by T_t changes (Figure 2A).

Location of UV lesions that disrupt reverse transcription

UV-induced damage of RNA is known to lead to lesions that stall reverse transcription and result in the production of cDNA that is truncated immediately upstream of the lesion. Analysis of the banding pattern produced from reverse transcription by using a fluorescently tagged primer therefore allows quantitative characterization of the damaged sites that interfere with reverse transcription.[26] We monitored reverse transcription of the MG aptamer after different times of exposure to UV. At time zero (no exposure), reverse transcription showed a single band in the polyacrylamide gel corresponding to the full-length cDNA (Figure 4A). However, exposure to UV light generated new bands over time, with a corresponding decrease in the intensity of the full-length cDNA band. The rate of decay of the full-length cDNA band matched well with the observed rate of functional decay (Figure 4B, cf. Figure 1A). To assign the position of damaged bases resulting in stalled cDNAs, reverse transcription was performed with 2′-3′-dideoxy bases (ddTTP, ddATP and ddGTP) and run alongside the damaged RNA. The highest degree of damage was noted for G24, U25, A31, U32, C37, and C38 (Figure 4C). Interestingly, the reactivity

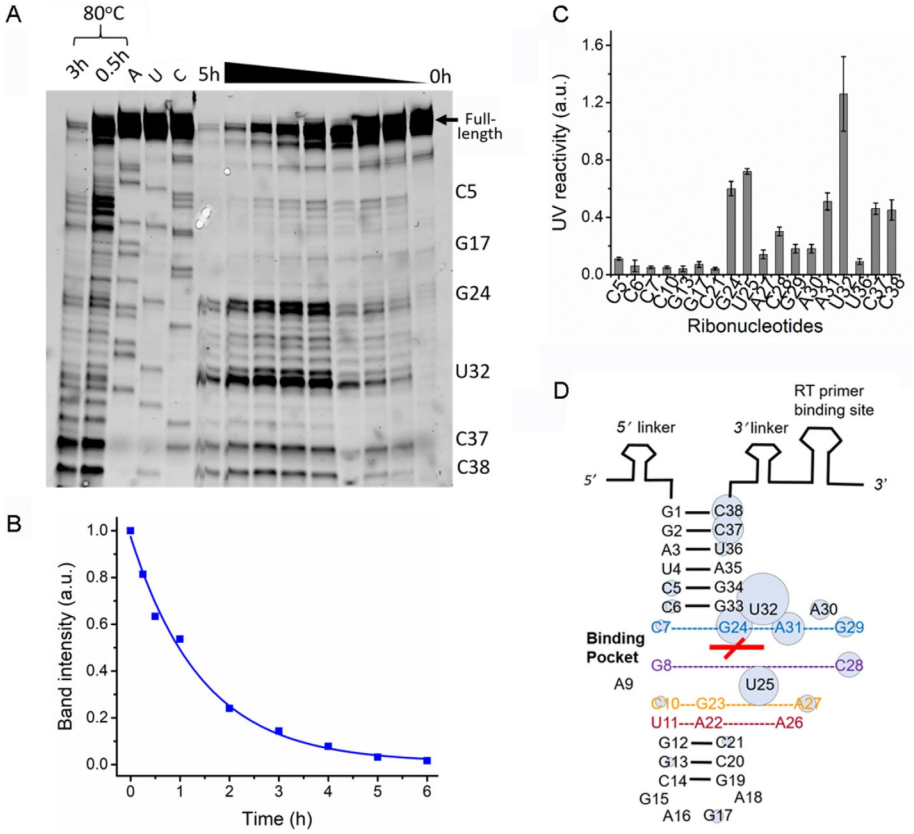

Figure 4. Characterization of damaged sites on the MG aptamer. A) Reverse transcription with a fluorescently tagged primer of RNA exposed to UV for various times (from right to left: 0, 0.5, 1, 2, 3, 4, 5 h) at room temperature was analyzed by PAGE. The lanes labeled A, U, and C correspond to sequencing reactions performed by using ddTTP, ddATP, and ddGTP as chain terminators, respectively. UV exposure was also carried out at 80 °C (left two lanes) for the times indicated. The site of damage is identified along the right side of the gel; the site listed is immediately downstream of the last nucleotide of the stalled DNA copy. B) Disappearance of full-length cDNA during UV exposure. The single-exponential decay has a rate constant of ≈0.8 h^{-1} (1.0 and 0.61 h^{-1} in two replicates). C) UV reactivity measured as the ratio of band intensity at a particular site divided by the band intensity of the full-length cDNA (R_i) after 4 h of exposure to UV. D) UV reactivity shown on the secondary structure of the MG aptamer in the context of the reverse transcription construct; the areas of the blue circles are proportional to the reactivity (see part (C)). The position of MG is shown in red.

of bases in the binding pocket appears to be higher than surrounding bases (Figure 4D). Of these, C37 and C38 are consistent with pyrimidine dimer formation. However, other possible pyrimidine dimers (positions C21, U11, and C5–7) were not noted to be particularly reactive at room temperature. In addition, stalling of reverse transcription at G24 and A31 indicates that purines are susceptible to a level of photodamage that is comparable to that of pyrimidines.

Sequence context is known to be an important influence on the reactivity of sites along functional RNA.[27] In order to deconvolute the influence of primary sequence versus RNA structure, we also exposed the MG aptamer to UV at 80 °C, well above its melting temperature. The exposure to high temperature would provide the level of reactivity associated with the primary sequence context, and the ratio of this to reactivity at room temperature would indicate the degree to which the UV reactivity of each site is affected by the folded structure. The rate of decay of the full-length transcript over UV exposure time was similar at 80 °C ($0.76 \pm 0.01\ h^{-1}$ at room temperature vs. $1 \pm 0.2\ h^{-1}$ at 80 °C; Figure 1B), thus indicating that temperature itself did not significantly alter the overall rate of damage. Bases within the binding pocket also exhibited no substantial change in reactivity upon melting. However, several sites were noted to increase substantially (more than fivefold) in reactivity with the change in temperature, namely C5, C6, C7, G13, C21, U36, and C38, and two sites (G34 and A35) showed damage at 80 °C but not at room temperature (Figures 5A and S2). These sites lie within or adjacent to stem structures.

If UV damage is assumed to occur on the RNA at random as a Poisson process, the probability of zero hits before a particular position n along the RNA is $e^{-h_n t}$, where h_n is the average number of hits before n per time. The probability of damage resulting in observation of a band at site n is then $p_n e^{-h_n t}$, where p_n is the probability of damage at site n. The probability of a molecule escaping damage, resulting in observation of a band at full-length reverse transcript, is e^{-Ht}, where the constant H is the average number of hits in the entire RNA per time. The disappearance of the full-length band was fit to a single exponential decay, yielding an H of approximately $0.8\ h^{-1}$ (Figure 4B). The average probability of a hit per site ($\overline{p_n}$) is thus $H/N \approx 0.01$ per site per hour, where $N = 77$ is the number of bases polymerized to produce a full-length reverse transcript. The ratio of band intensity at site n to band intensity of the full-length transcript is $R_I(n) = p_n e^{(H-h_n)t}$. As $h_n < H$, the exponent has a positive absolute value. This simple Poisson model suggests that R_I could be fit to an exponential function with respect to time. Indeed, the observed $R_I(n)$ curves could be fit well by an exponential Equation (1):

$$R_I = R_{I,0} + Be^{\lambda t} \quad (1)$$

where $R_{I,0}$ is the baseline ratio (Figures 5B–E and S3; Table 1). Higher λ reflects more rapid accumulation of damage at that

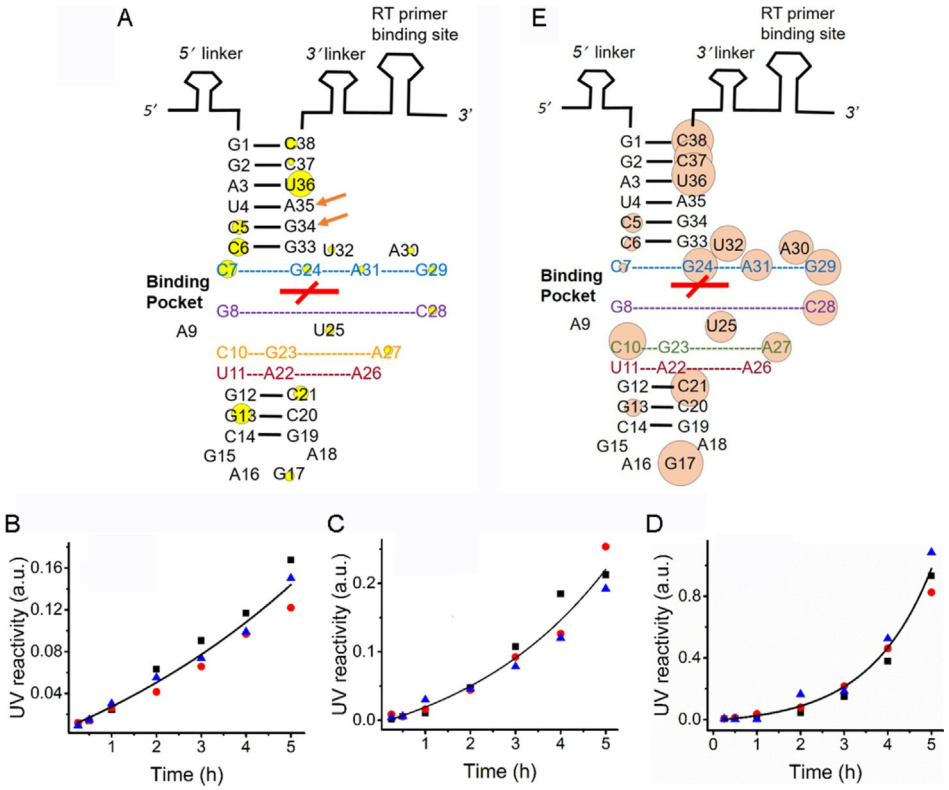

Figure 5. UV reactivity and structural elements of the MG aptamer. A) Relative increase in UV reactivity upon heat denaturation. The areas of the yellow circles are proportional to the ratio of UV reactivity at 80 °C to room temperature (both taken at 0.5 h; see data in Figure S2). Orange arrows indicate sites where UV reactivity was observed at 80 °C but not room temperature. UV reactivity (R_I) over time for sites B) C5, C) A27, and D) C38, determined by reverse-transcription gel assay, chosen as examples of various rates of reactivity ($\lambda = 0.15$, 0.37, and $0.72\ h^{-1}$, respectively; Table 1). Each color represents a different replicate. E) λ for each site, with the area of the orange circle proportional to λ.

Table 1. Rate of exponential increase (λ) in UV reactivity for sites of the MG aptamer. Standard deviations are calculated from replicates.

Aptamer position	λ [h^{-1}]	Aptamer position	λ [h^{-1}]
C5	0.15 ± 0.04	C6	0.08 ± 0.01
C7	0.04 ± 0.02	C10	0.60 ± 0.10
G13	0.12 ± 0.02	G17	0.85 ± 0.38
C21	0.60 ± 0.14	G24	0.50 ± 0.09
U25	0.40 ± 0.11	A27	0.37 ± 0.14
C28	0.50 ± 0.16	G29	0.52 ± 0.13
A30	0.47 ± 0.09	A31	0.41 ± 0.13
U32	0.52 ± 0.14	U36	0.80 ± 0.20
C37	0.61 ± 0.06	C38	0.72 ± 0.16

position. h_n can also be estimated from λ. h_n is expected to increase with n, and this is indeed observed as an overall trend with slope similar to the average probability of damage per site (H/N; Figure S4).

This analysis is advantageous in combining data from multiple time points and controlling for sources of band intensity that are unrelated to reactivity, and should thus lead to a more accurate estimate of reactivity compared to a single time point (compare with Figure 4C, D). Consistent with the analyses above, in addition to sites of potential pyrimidine dimer formation, the aptamer binding pocket is particularly prone to UV-induced damage.

Discussion

UV exposure creates chemical lesions, but not all of these lesions will affect the activity of the RNA. We exposed two RNA aptamers to UV light and then measured their ability to bind the respective ligand. Loss of activity upon UV exposure was observed to follow single-exponential decay, with the rate constant differing for the two aptamers. Damage at a small number of important sites appears to mediate loss of activity, based on two observations. First, the apparent K_D of both aptamers was not substantially affected by UV exposure, even as the total fluorescence decreased to low levels, thus suggesting that complexes that retained fluorescence were not severely hampered by UV damage. Second, although the fluorescence of the MG aptamer decayed to near background levels, the Spinach2 aptamer retained ≈25% fluorescence after long exposures. A possible explanation could be that a particular lesion at a critical site causes loss of fluorescence, but this site is protected if a different lesion occurs first; alternatively, there might exist an equilibrium with self-repair[28] at the critical site of damage. Interestingly, although ssRNA and dsRNA are known to exhibit different rates of damage accumulation,[17] denatured MG aptamer exhibited a similar loss of activity to folded MG aptamer. The damage in the dye-binding pocket might or might not also affect its local structural stability (measured by T_t), depending on the aptamer, and the stability of the overall secondary structure (measured by T_m) did not appear to be sensitive to UV exposure. These findings suggest that damage resulting in deactivation occurs at a small number of critical single-stranded regions (e.g., the dye-binding pocket), whereas damage elsewhere is largely functionally inconsequential.

A second important aspect of activity for functional RNA in the RNA World is its ability to act as a template for replication. We measured the ability of reverse transcriptase to synthesize a full-length cDNA from the MG aptamer, and found that it decays on a timescale similar to functional decay upon UV exposure. Reverse transcription stalls at chemical lesions, including pyrimidine dimers.[20,27] Some of the stalled products indicated damage at potential pyrimidine dimer sites, but not all potential sites appeared to be damaged. This is consistent with the strong dependence of UV susceptibility on local structural context. For example, the presence of flanking GC base pairs might hinder the flexibility of the duplex, which is needed for photolesion formation.[16] In addition, certain purine sites caused stalling, thus indicating other types of damage (e.g., photo-oxidation). The binding pocket of the MG aptamer appeared to be most prone to UV damage, in contrast to the tetraloop region, which was only slightly susceptible, despite being single-stranded. We noted that denaturation did not affect the rate of overall loss of fluorescence of the MG aptamer, but that assay would not necessarily be sufficiently sensitive to detect changes in the rate of damage to individual lesions. Although overall fluorescence is presumably influenced by multiple sites, some of which are not affected by denaturation, assaying individual lesions could potentially identify those sites specifically affected by denaturation. Indeed, we found that the pattern of lesions was altered for denatured aptamer. Although there was little change to the binding pocket, which still exhibited the greatest damage, or to the tetraloop, sites in the stem structures exhibited greater susceptibility to damage when denatured; this suggested that formation of the duplex in the folded structure is protective against UV-induced lesions. A caveat is that denaturation in this study was carried out by heating to 80 °C, and it is possible that unusually stable structures might not be completely disrupted at this temperature; therefore, we might underestimate the extent to which folding affects UV susceptibility. Similarly, although the overall rate of loss of fluorescence of the MG aptamer was not substantially affected whether irradiated in the presence of absence of MG, it is possible that the rate of chemical damage at specific sites could be affected, particularly given the induced fit of the aptamer to its ligand;[23a] further work would be necessary to characterize this aspect of the system.

To better quantify the rate of damage detected by the reverse-transcription assay, we noted that the kinetic data fit well to a Poisson model of damage. Although a Poisson model has clear inaccuracies (e.g., the assumption of independent hits is violated in the case of pyrimidine dimers), it was used to suggest a functional form for fitting the quantitative data. Empirically, the increase in the ratio between a stalled product and the full-length cDNA matched well to the exponential form predicted, thus allowing the rate of damage to be estimated from kinetic data (Figure 5E) rather than amount of damage at a single time point (Figure 4C, D). Kinetic analysis might be useful, as the rates are expected to be less prone to artifacts from bands unrelated to UV damage, more accurate due to

the contributions of several data points, and more easily comparable across different sequences. The findings from this analysis were consistent with the increased susceptibility of the binding pocket, and also verified sites of damage in the tetraloop and at pyrimidine dimers in the stem. It is important to note that the reverse transcription assay might not be sensitive to all chemical lesions, depending on the properties of the enzyme. Confirmation of their chemical nature would require other analysis, such as mass spectrometry.[16]

The structure of the MG aptamer[23a] indicates that the binding pocket does not contain potential sites for pyrimidine dimer formation. Nevertheless, our analysis identifies G24, A31, and G29 as sites of relatively rapid damage ($\lambda > 0.4\ h^{-1}$; Table 1). These three bases are part of a base quadruple that stacks against the MG ligand in the binding pocket. In addition, C28, which forms part of a Watson–Crick base pair that stacks on the other side of MG, is also damaged rapidly ($\lambda = 0.5\ h^{-1}$). Damage at these sites might directly disrupt binding and cause a loss of fluorescence. In addition, although U25 and A27 do not contact MG directly, they stabilize the binding pocket, and mutation of these residues greatly decreases affinity.[23a] As U25 and A27 are also sites of notable damage ($\lambda \approx 0.4\ h^{-1}$), these could also contribute to the observed loss of fluorescence upon UV irradiation. On the other hand, the binding pocket of the Spinach2 aptamer[23c] does contain potential sites for pyrimidine dimers at U61–U62 (equivalent to U50–U51 in construct 24-2-min used for structural characterization) and U32–C33–C34 (equivalent to U29–C30–C31 in 24-2-min). Both U61 and U32 participate in a Hoogsteen base triple that stacks against the ligand. U32 is an intriguing site in light of the observation that substantial fluorescence remains after long UV exposures; one might speculate that formation of the U32–C33 dimer competes with formation of the C33–C34 dimer, leaving U32 intact in some fraction of molecules; further experimental work would be needed to test this hypothesis. Although one might assume that the U61–U62 sequence could lead to rapid disruption of the binding site by UV damage, the affinity of Spinach2 is only modestly perturbed by 2′-deoxy modification of U61,[23c] whose 2′-OH normally contacts the ligand. In addition, a large part of the Spinach2 binding site is formed by a G-quadruplex structure whose critical residues would not form pyrimidine dimers, although they could be sensitive to photo-oxidative damage. Compared to the MG aptamer, these differences might contribute to the observed retention of substantial fluorescence (Figure 1A) and thermodynamic stability (Figure 2C) by the Spinach2 aptamer during UV exposure.

UV irradiation of the RNA aptamers studied here is consistent with both the known increased susceptibility of single-stranded regions to damage[17] and the sensitivity of damage rates to precise molecular context.[16] Although we studied exposure under total photon fluences similar to those of the surface of the early Earth, the spectrum was limited (258–274 nm), giving a relatively high intensity in a narrow range compared to the sun. As excited-state lifetimes depend on wavelength, a broad-spectrum source might give more realistic results. We note a generally increased susceptibility of the binding pocket compared to the stems, but there is also large variation among seemingly similar sites. In the context of the RNA World, the protective effect of stem structures might favor the evolution of well-folded functional RNA compared to sequences with more disordered folds. Overall, the lifetime of the MG aptamer, in terms of both functional activity and templating ability, might be 1–2 hours under conditions similar to those used here. However, some sequences, such as the Spinach2 aptamer, appear to be able to withstand substantial UV exposure, retaining function for more than several hours through an unknown mechanism. UV hardiness might also be influenced by self-repair[28] or by repair ribozymes or deoxyribozymes.[29] Although it is at present difficult to predict the relationship between sequence and UV hardiness, the results here indicate that sequences can vary by orders of magnitude in this component of fitness. This work highlights the importance of considering UV exposure as one of the selective pressures shaping the fitness landscape of RNA[30] during prebiotic evolution.

Experimental Section

Materials: Malachite green (MG) chloride (Sigma–Aldrich), DFHBI 1T (Tocris), bicine (Alfa Aesar), GlycoBlue (Invitrogen), and SYBR gold (Invitrogen) were used as received. The MG RNA aptamer (5′-GGAUC CCGAC UGGCG AGAGC CAGGU AACGA AUGGA UCC-3′) and other oligonucleotides were obtained by chemical synthesis and HPLC-purified by Integrated DNA Technologies (IDT). The Spinach2 aptamer and MG aptamer construct for reverse transcription study was prepared by in vitro transcription. Chemicals not mentioned above were purchased from Fisher Scientific.

Aptamer synthesis: The DNA template sequence of the Spinach2 RNA aptamer (5′-CTTTA CCCGA GTGTA ATACG ACTCA CTATA GGGAG AGATG TAACT GAATG AAATG GTGAA GGACG GGTCC AGTAG GCTGC TTCGG CAGCC TACTT GTTGA GTAGA GTGTG AGCTC CGTAA CTAGT TACAT CCTAG CATAA CCCCT TGGGG CCTCT AAACG GGTCT TGAGG GGTTT TTTGC CCACG GTAAA C-3′; aptamer region underlined) was PCR amplified by KAPA Taq ReadyMix PCR Kit (KAPA Biosystems) using primers (forward: CTTTA CCCGA GTGTA ATACG ACTCA CTATA GGGAG AGATG TAACT GA, reverse: GTTTA CCGTG GGCAA AAAAC CCCTC AAGAC C) that introduce a T7 promoter sequence at the 5′-end and an additional 60 nucleotides at the 3′-end for transcription termination. The RNA product of 155 nt was gel purified (8% native-PAGE). In vitro transcription of the Spinach2 RNA was performed by HiScribe T7 Quick High Yield RNA synthesis kit (New England Biolabs, Massachusetts). Both the PCR and transcription products were gel extracted by the "crush and soak" method followed by ethanol precipitation for 1 h at −20 °C and centrifuged at 20000 *g* and 4 °C for 60 min. The supernatant was removed, and pellets were rinsed with 70% cold ethanol (2× 1 mL), dried in air for 2 h, and resolubilized in RNase-free deionized water.

UV irradiation of RNA: The RNA samples were exposed for various lengths of time to UV light (either at room temperature or 80 °C) with a Fluoromax 4C instrument from Horiba, which contains a xenon lamp source and monochromator. The excitation wavelength was 266 nm (bandpass = 16 nm used unless otherwise noted), and the rate of exposure was measured to be approximately 2 $mJ\,cm^{-2}\,s^{-1}$ with a Newport 842-PE power meter connected with 818-UV photodetector sensor. This flux is equivalent to ≈2.7×

10^{15} photons $cm^{-2} s^{-1}$. Lower fluence was achieved by reducing the bandpass width. The RNA aptamer solution (~3.4 μM in 200 μL of 10 mM Tris·Cl, pH 8.5) was heated to 90 °C for 3 min and cooled on ice for 10 min. The cooled RNA was diluted with buffer and salt solution so as to obtain a final concentration of 0.2 μM RNA in 0.6 mM Tris, 10 mM HEPES, 1 mM Mg citrate, 100 mM KCl, 0.2 M bicine (pH 8.5). The time-dependent fluorescence change of an aptamer was fit by an exponential Equation (2):

$$F = F_0 + Ae^{-k_f t} \quad (2)$$

where F is the fluorescence, A is a pre-exponential factor, k_f is the rate constant of fluorescence decrease and t is the time of exposure. Encapsulation of the MG aptamer in POPC vesicles was performed as described previously.[25]

Polyacrylamide gel electrophoresis of UV-damaged RNA: The UV-treated RNA samples were precipitated by adding $^1/_{10}$th volume of sodium acetate (pH 5.4), GlycoBlue (15 μg) and three volumes of cold ethanol (taken out of −20 °C storage). The samples were cooled at −20 °C for 1 h before centrifuging at 20000 *g* for 1.5 h. The pellets were washed twice with 70% cold ethanol and vacuum dried for 1 h. The pellet was dissolved in water and heat-treated at 90 °C for 3 min, cooled on ice for 15 min, and refolded by adding buffer and salt solution (2 mM Tris, 10 mM HEPES, 1 mM Mg citrate, 100 mM KCl, 0.2 M bicine (pH 8.5)). For native PAGE, the annealed RNA was mixed with 6× gel loading dye (NEB) before being loaded onto a 10% native gel (acrylamide: bisacrylamide (29:1)). Gels were run at 325 V for 1 h in 1× TBE buffer and stained by SYBR gold. The gel was scanned on an Amersham Typhoon 5.

For denaturing PAGE, RNA samples were heat-denatured at 90 °C for 5 min in 1× urea gel loading buffer (National Diagnostics), cooled on ice for 10 min, and loaded on an 8% polyacrylamide gel (acrylamide/bisacrylamide (29:1)) containing 7.5 M urea. Gels were run and stained as described above.

Dissociation constant (K_D) measurement: The steady-state emission intensity of the dye-bound RNA aptamer (MG or Spinach2) was measured by using the TECAN M200 Pro plate reader. The UV-treated RNA aptamer (0.15 μM, exposed for various length of time) was mixed with different known concentrations of ligands (MG or DFHBI 1T), and fluorescence was monitored at the appropriate wavelength (λ_{ex} = 617 nm, λ_{em} = 655 nm for MG; λ_{ex} = 440 nm and λ_{em} = 505 nm for DFHBI 1T). Fluorescence intensity was normalized to a minimum of 0 and a maximum of 1 and plotted for binding curve analysis. The curve fitting was performed in Origin Pro 9 software according to the analytical quadratic solution[31] [Eq. (3)]:

$$\frac{F}{F_{max}} = \frac{C + K_D + R - \sqrt{(C + K_D + R)^2 - 4CR}}{2} \quad (3)$$

where F is the fluorescence, C is the concentration of ligand, K_D is the dissociation constant and R is the aptamer concentration. The reported K_D is the average of three independent experiments.

Melting transitions of RNA measured by fluorescence: The fluorescence of the MG aptamer was measured at different temperatures by using a Fluoromax 4C (Horiba) with a Peltier-controlled temperature attachment (Model F-3004, Horiba). The RNA aptamer was UV treated for 6 h before dye addition. The fluorescence of the aptamer·dye complex (0.2 μM MG RNA and 15 μM MG dye) was recorded in 3 °C increments from 1 to 70 °C, with 10 min of incubation at each interval. Fluorescence intensities (λ_{ex} = 617 nm, λ_{em} = 655 nm) were recorded and plotted after normalization to minimum of 0 and a maximum of 100. Melting curves were fit in Origin Pro 9 software by using the Boltzmann sigmoidal Equation (4):

$$F = F_{min} + \frac{(F_{max} - F_{min})}{1 + \exp((T_t - T)/s)} \quad (4)$$

where F refers to fluorescence and F_{min} and F_{max} are the minimum and maximum fluorescence, respectively, T is temperature, T_t is the transition temperature, and s is a fitting parameter. T_t values presented here are average of three independent experiments. For Spinach2, 0.2 μM aptamer was irradiated for 6 h, and 0.1 μM aptamer RNA + 50 μM DFHBI 1T was subjected to the melting study as described for the MG aptamer.

Melting curve of RNA by circular dichroism spectroscopy: Temperature-dependent CD spectra were acquired on a JASCO J-1500 spectrophotometer (JASCO International Co. Ltd, Tokyo, Japan) equipped with a Peltier-controlled cell holder (model PTC-517, JASCO). A sample containing 0.2 μM RNA, 2.5 mM Tris, 10 mM HEPES, 1 mM Mg citrate, and 100 mM KCl in 0.2 M bicine (pH 8.5) was prepared. After UV treatment for 6 h, the samples were ethanol precipitated and refolded in aqueous buffer containing 2 mM Tris, 10 mM HEPES, 1 mM Mg citrate, and 100 mM KCl in 0.2 M bicine (pH 8.5). The CD signal of the concentrated (~52.6 ng μL^{-1}) aptamer was monitored at 264 nm in 5 °C increments from 1 to 91 °C, with 10 min of incubation at each interval. The spectra were recorded by using a 1 mm path-length cuvette. Melting curves were fit in Origin Pro 9 software by using the Boltzmann sigmoidal Equation (5):

$$\theta = \theta_{min} + \frac{\theta_{max} - \theta_{min}}{1 + \exp((T_m - T)/s)} \quad (5)$$

where θ refers to the ellipticity at 264 nm and θ_{min} and θ_{max} are the minimum and maximum θ, respectively, T is temperature, T_m is the melting temperature, and s is a fitting parameter.

Reverse transcription assay for UV damage: The RNA used for the reverse transcription assay was generated from a DNA template (aptamer region in bold text): 5′-TAATA CGACT CACTA TAGGG CCTTC GGGCC AA**GGA TCCCG ACTGG CGAGA GCCAG GTAAC GAATG GATCC** TCGAT CCGGT TCGCC GGATC CAAAT CGGGC TTCGG TCCGG TTC-3′). This sequence contains a T7 promoter, 5′ and 3′ linker regions, and a 3′ reverse transcription (RT) primer binding site, as previously described.[25] The 5′ and 3′ flanking sequences of 14 and 43 nucleotides allow every base of the MG aptamer to be evaluated in a sequencing gel. The ssDNA template was obtained from IDT and amplified through 30 cycles of PCR by using KAPA Taq ReadyMix PCR kit (Kapa Biosystems) in a Bio-Rad C1000 thermal cycler (forward primer sequence: 5′-TAATA CGACT CACTA TAGGG CCTTC GG-3′; reverse primer sequence: 5′-GAACC GGACC GAAGC CCG-3′). Transcription was performed by using the HiScribe T7 Quick High Yield RNA Synthesis Kit (NEB) as previously described.[25] Reverse transcription reactions were conducted as follows: irradiated RNA (10 μL) concentrated after ethanol precipitation (or 1 μL of 143 μM transcript for sequencing reactions), reverse primer (2 μL, 2 μM), and dNTP mix (1 μL, 10 μM) were mixed, and the mixture was incubated at 65 °C for 5 min, then annealed on ice for 5 min. Superscript IV buffer mix (4 μL), dithiothreitol (1 μL, 0.1 M), and Superscript IV reverse transcriptase (1 μL) were added, and the reaction mixture was incubated at 55 °C for 10 min, and then inactivated at 80 °C for 10 min. RNA was removed by base hydrolysis through the addition of NaOH (1 μL, 4 M) followed by neutralization by Tris·HCl (4 μL, 1 M). Samples were analyzed by 12%

urea-PAGE run on an Apogee S2 sequencing gel apparatus at 1200 V for 6 h. The gel was imaged by using an Amersham Typhoon 5 (GE), and band quantitation was performed by using GE ImageQuant software. The RT primer was fluorescently labeled at the 5′-end with Rhodamine Green to allow detection of bands on the gel (RT Primer sequence:/5RhoG-XN/GAACC GGACC GAAGC CCG). The ratio of band intensity for a particular base to the band intensity of the full-length reverse transcript (R_I) within the same lane was measured.

Acknowledgements

We thank Mattanjah de Vries, Dimitar Sasselov, Dieter Braun, and Christof Mast for helpful discussions. Funding was provided by the Simons Foundation (grants 290356 and 481325) and NASA (NNX16AJ32G).

Conflict of Interest

The authors declare no conflict of interest.

Keywords: biological chemistry · chemical biology · functional RNA aptamers · prebiotic evolution · UV damage

[1] a) W. Gilbert, *Nature* **1986**, *319*, 618; b) G. F. Joyce, *Nature* **2002**, *418*, 214 – 221; c) A. Pressman, C. Blanco, I. A. Chen, *Curr. Biol.* **2015**, *25*, R953 – R963.
[2] a) M. W. Powner, B. Gerland, J. D. Sutherland, *Nature* **2009**, *459*, 239 – 242; b) B. H. Patel, C. Percivalle, D. J. Ritson, C. D. Duffy, J. D. Sutherland, *Nat. Chem.* **2015**, *7*, 301 – 307; c) M. W. Powner, J. D. Sutherland, *ChemBioChem* **2008**, *9*, 2386 – 2387; d) J. Xu, M. Tsanakopoulou, C. J. Magnani, R. Szabla, J. E. Sponer, J. Sponer, R. W. Gora, J. D. Sutherland, *Nat. Chem.* **2017**, *9*, 303 – 309.
[3] P. K. Sarker, J. Takahashi, Y. Kawamoto, Y. Obayashi, T. Kaneko, K. Kobayashi, *Int. J. Mol. Sci.* **2012**, *13*, 1006 – 1017.
[4] C. Bonfio, L. Valer, S. Scintilla, S. Shah, D. J. Evans, L. Jin, J. W. Szostak, D. D. Sasselov, J. D. Sutherland, S. S. Mansy, *Nat. Chem.* **2017**, *9*, 1229 – 1234.
[5] S. Ranjan, D. D. Sasselov, *Astrobiology* **2016**, *16*, 68 – 88.
[6] I. Cnossen, J. Sanz-Forcada, F. Favata, O. Witasse, T. Zegers, N. Arnold, *J. Geophys. Res.* **2007**, *112*, E02008.
[7] a) M. J. Janicki, S. J. Roberts, J. Sponer, M. W. Powner, R. W. Gora, R. Szabla, *Chem. Commun.* **2018**, *54*, 13407 – 13410; b) C. Sagan, *J. Theor. Biol.* **1973**, *39*, 195 – 200; c) S. J. Roberts, R. Szabla, Z. R. Todd, S. Stairs, D. K. Bucar, J. Sponer, D. D. Sasselov, M. W. Powner, *Nat. Commun.* **2018**, *9*, 4073.
[8] E. J. Wurtmann, S. L. Wolin, *Crit. Rev. Biochem. Mol. Biol.* **2009**, *44*, 34 – 49.
[9] K. Heil, D. Pearson, T. Carell, *Chem. Soc. Rev.* **2011**, *40*, 4271 – 4278.
[10] C. Zwieb, A. Ross, J. Rinke, M. Meinke, R. Brimacombe, *Nucleic Acids Res.* **1978**, *5*, 2705 – 2720.
[11] R. P. Rastogi, Richa, A. Kumar, M. B. Tyagi, R. P. Sinha, *J. Nucleic Acids* **2010**, *2010*, 592980.
[12] a) S. Boldissar, M. S. de Vries, *Phys. Chem. Chem. Phys.* **2018**, *20*, 9701 – 9716; b) A. A. Beckstead, Y. Zhang, M. S. de Vries, B. Kohler, *Phys. Chem. Chem. Phys.* **2016**, *18*, 24228 – 24238.
[13] A. Abo-Riziq, L. Grace, E. Nir, M. Kabelac, P. Hobza, M. S. de Vries, *Proc. Natl. Acad. Sci. USA* **2005**, *102*, 20 – 23.
[14] M. Pearson, H. E. Johns, *J. Mol. Biol.* **1966**, *20*, 215 – 229.
[15] B. Singer, *Virology* **1971**, *45*, 101 – 107.
[16] L. M. Kundu, U. Linne, M. Marahiel, T. Carell, *Chem. Eur. J.* **2004**, *10*, 5697 – 5705.
[17] Z. Qiao, Y. Ye, P. H. Chang, D. Thirunarayanan, K. R. Wigginton, *Environ. Sci. Technol.* **2018**, *52*, 10408 – 10415.
[18] T. Gustavsson, R. Improta, D. Markovitsi, *J. Phys. Chem. Lett.* **2010**, *1*, 2025 – 2030.
[19] T. V. Ramabhadran, J. Jagger, *Proc. Natl. Acad. Sci. USA* **1976**, *73*, 59 – 63.
[20] M. S. Iordanov, D. Pribnow, J. L. Magun, T. H. Dinh, J. A. Pearson, B. E. Magun, *J. Biol. Chem.* **1998**, *273*, 15794 – 15803.
[21] a) R. E. Wellinger, F. Thoma, *EMBO J.* **1997**, *16*, 5046 – 5056; b) H. Gaillard, D. J. Fitzgerald, C. L. Smith, C. L. Peterson, T. J. Richmond, F. Thoma, *J. Biol. Chem.* **2003**, *278*, 17655 – 17663.
[22] E. Biondi, S. Branciamore, M. C. Maurel, E. Gallori, *BMC Evol. Biol.* **2007**, *7*, S2.
[23] a) J. Flinders, S. C. DeFina, D. M. Brackett, C. Baugh, C. Wilson, T. Dieckmann, *ChemBioChem* **2004**, *5*, 62 – 72; b) C. Baugh, D. Grate, C. Wilson, *J. Mol. Biol.* **2000**, *301*, 117 – 128; c) H. Huang, N. B. Suslov, N. S. Li, S. A. Shelke, M. E. Evans, Y. Koldobskaya, P. A. Rice, J. A. Piccirilli, *Nat. Chem. Biol.* **2014**, *10*, 686 – 691; d) J. S. Paige, K. Y. Wu, S. R. Jaffrey, *Science* **2011**, *333*, 642 – 646; e) R. L. Strack, M. D. Disney, S. R. Jaffrey, *Nat. Methods* **2013**, *10*, 1219 – 1224.
[24] W. Song, R. L. Strack, N. Svensen, S. R. Jaffrey, *J. Am. Chem. Soc.* **2014**, *136*, 1198 – 1201.
[25] R. Saha, S. Verbanic, I. A. Chen, *Nat. Commun.* **2018**, *9*, 2313.
[26] X. Gong, R. Tao, Z. Li, *Anal. Biochem.* **2006**, *357*, 58 – 67.
[27] W. Kladwang, J. Hum, R. Das, *Sci. Rep.* **2012**, *2*, 517.
[28] a) D. B. Bucher, C. L. Kufner, A. Schlueter, T. Carell, W. Zinth, *J. Am. Chem. Soc.* **2016**, *138*, 186 – 190; b) R. Szabla, H. Kruse, P. Stadlbauer, J. Sponer, A. L. Sobolewski, *Chem. Sci.* **2018**, *9*, 3131 – 3140.
[29] a) A. Barlev, D. Sen, *Acc. Chem. Res.* **2018**, *51*, 526 – 533; b) A. Barlev, G. S. Sekhon, A. J. Bennet, D. Sen, *Biochemistry* **2016**, *55*, 6010 – 6018; c) D. J. Chinnapen, D. Sen, *Proc. Natl. Acad. Sci. USA* **2004**, *101*, 65 – 69.
[30] S. S. Athavale, B. Spicer, I. A. Chen, *Curr. Opin. Chem. Biol.* **2014**, *22*, 35 – 39.
[31] T. D. Pollard, *Mol. Biol. Cell* **2010**, *21*, 4061 – 4067.

Manuscript received: April 20, 2019
Accepted manuscript online: May 24, 2019
Version of record online: August 21, 2019

